J Infrared Milli Terahz Waves (2014) 35:118–130
DOI 10.1007/s10762-013-0004-5

Terahertz Imaging System for Medical Applications and Related High Efficiency Terahertz Devices

Toshihiko Ouchi · Kousuke Kajiki · Takayuki Koizumi · Takeaki Itsuji · Yasushi Koyama · Ryota Sekiguchi · Oichi Kubota · Kodo Kawase

Received: 1 May 2013 / Accepted: 8 July 2013 /
Published online: 20 July 2013

Abstract A terahertz (THz) imaging system and high efficient terahertz sources and detectors for medical applications were developed. A fiber laser based compact time domain terahertz tomography system was developed with a high depth resolution of less than 20 μm. Three-dimensional images of porcine skin were obtained including some physical properties such as applied skin creams. The discrimination between healthy human tissue and tumor tissue has been achieved using reflection spectra.

To improve the THz imaging system, a ridge waveguide $LiNbO_3$ based nonlinear terahertz generator was studied to achieve high output power. A ridge waveguide with 5-7 μm width was designed for high efficiency emission from the $LiNbO_3$ crystal by the electro-optic Cherenkov effect.

Terahertz electronic sources and detectors were also realized for future imaging systems. As electronic source devices, resonant tunneling diode (RTD) oscillators with a patch antenna were fabricated using an InGaAs/InAlAs/AlAs triple barrier structure. On the other side, Schottky barrier diode (SBD) detectors with a log-periodic antenna were fabricated by thin-film technology on a Si substrate. Both devices operate above 1 THz at room temperature. This electronic THz device set could provide a future high performance imaging system.

Keywords Terahertz (THz) · Medical imaging · Time domain spectroscopy (TDS) · Resonant tunneling diode (RTD) oscillator · Schottky barrier diode (SBD) detector

1 Introduction

In the past decade, the generation and detection of broadband terahertz (THz) pulses have been studied using various approaches. Generation by optical rectification and detection by electro-optic sampling using nonlinear crystals are one of the typical methods [1, 2]. Photoconductive

T. Ouchi (✉) · K. Kajiki · T. Koizumi · T. Itsuji · Y. Koyama · R. Sekiguchi · O. Kubota
Corporate R&D, Canon Inc., 3-30-2 Shimomaruko, Ohta-ku, Tokyo 146-8501, Japan
e-mail: ouchi.toshihiko@canon.co.jp

K. Kawase
EcoTopia Science Institute, Nagoya University, Furo-cho, Chikusa-ku, Nagoya 464-8603 Nagoya, Japan

switches (PCSs) based on low temperature grown (LT) GaAs are also employed as emitters [3] and detectors [4]. THz time-domain spectroscopy (THz-TDS) using these broadband THz waves is attractive for non-destructive inspection systems [5]. Biomedical tissue imaging by THz pulses, such as cancer diagnosis, could be important applications [6]. As THz radiations do not affect human tissue because of their low energy, THz imaging is expected to become a new modality of medical imaging as a noninvasive diagnosis. Indeed a lot of reports on the possibility of tissue discrimination without staining were made recently [7–10].

For high speed medical imaging, higher THz radiation power will be required to overcome the high absorption of the tissue. Recently, several high output power generators based on nonlinear optics were reported [11]. However, ordinary nonlinear generator requires ultra-high power excitation lasers using regenerative amplifier for TDS systems. To establish a compact and stable fiber laser based TDS system, a waveguide type nonlinear generator using the electro-optic Cherenkov effect [12] could be useful. For high conversion efficiency, a ridge waveguide type generator was suitable to obtain high optical density [13].

Furthermore, THz electronic sources and detectors were also realized for future compact innovative imaging systems. Semiconductor based THz oscillators like semiconductor lasers, quantum cascade lasers (QCLs) [14] and resonant tunneling diodes (RTDs) [15] have been studied extensively. Oscillations characteristics such as output power, oscillation frequency, and operating temperature are improving rapidly. Besides these oscillators with fundamental operation in the THz range, up-conversion techniques using lower frequencies and frequency multiplication amplifiers can provide sub-terahertz emission. Sub-terahertz amplifiers have been achieved using heterojunction bipolar transistors (HBTs) [16, 17], and the monolithic integration of SiGe HBTs showed over 0.3 THz output using a frequency multiplier chain [18].

These solid-state devices are expected to be small and highly efficient THz sources in the near future. Especially, RTD based oscillators are attractive due to their room temperature (R.T.) fundamental oscillations. Above 1.0 THz oscillations have been reported using InGaAs/AlAs double-barrier RTD on slot antenna [19, 20], and with slot-antenna resonators and planar Vivaldi antennas on dielectric membrane [21]. Triple-barrier RTDs with integrated patch antenna, which are capable of surface-emission, were also reported [22, 23].

Similarly, semiconductor based detectors are also extensively studied aiming at THz focal plane imagers. Schottky barrier diodes (SBDs) [24–28] are one of the popular THz detectors due to the following points: they operate at room temperature and they have a high-speed and high efficient response which can improve the detector's performance using RF technology such as modulation techniques. Antenna coupled SBD detector for THz frequency range has been proposed in 1975 [24]. Scanning THz Imaging was performed with GaAs SBD detector using heterodyne detection [25]. Direct detection with an order of $pW/Hz^{1/2}$ noise equivalent power (NEP) was predicted and achieved employing an InGaAs/InAlAs low barrier SBD with integrated planar antennas [26]. A 0.8-THz detection with excellent NEP of 20 $pW/Hz^{1/2}$ was reported in [27].

Recently plasmon-resonant or plasmon-damped detection using semiconductor transistors has also become promising for THz detectors. The HENT device has very high sensitivity as well as low noise equivalent power [29]. Si CMOS based plasmon detectors have demonstrated practical characteristics as two dimensional imagers although response frequency is lower than 1 THz [30]. Up to 4.3 THz detection by CMOS devices was demonstrated recently with a patch antenna [31]. A combination of CMOS and Schottky barrier diodes was also studied [32]. Thus, semiconductor based THz imaging devices are getting extensively studied in the world.

This paper describes our recent progresses in THz-TDS imaging systems with highly efficient generators for medical applications as well as solid-state THz sources and detectors.

2 Terahertz TDS Imaging System

2.1 THz-TDS and its medical application

We are developing a fiber laser based compact TDS system and studying its medical applications. Figure 1 shows the experimental set up of a THz imaging system based on the conventional TDS [5]. An ultra-short pulse fiber laser with 30-fs pulse duration and an LT-InGaAs photoconductive switch (PCS) emitter which operates at 1.55 μm wavelength were prepared.

In order to operate the LT-GaAs PCS detector, a split beam was input to the periodically poled lithium niobate (PPLN: thickness 0.1 mm, 100 °C) to generate 780-nm pulses. The obtained terahertz radiation was a monocycle-like pulse of 350 fs duration with flat frequency distribution up to 4.5 THz at 30 mW pump power and 1 mW probe power condition. This system operates as a tomography imaging system with a depth resolution of less than 20 μm.

We applied this imaging system for biomedical tissue observation. Skin monitoring such as 3-dimesional tomography of dermis and epidermis with stratum corneous is useful for medical imaging. For example, in-vivo or non-pathological imaging is desirable for the diagnosis of tumors, inflammations, etc. [8].

Figure 2 shows an example of 3-dimesional image of a sliced porcine skin to which skin cream was partially applied. The boundary of dermis and epidermis was clearly observed in an expanded cross sectional view. In the epidermis layer, we could recognize uneven structures which had differences according to the presence of cream. That was a demonstration of a component analysis under skin which leads to fundamental experiments for drug delivery systems.

Tumor diagnosis is one of the important future applications for THz imaging. We measured the reflection characteristics of colorectal cancer. The samples were non-stained blocks of tissue prepared by formalin fixation and paraffin embedding. Reflectance spectra calculated from THz-TDS measurement data of tumor area and normal area are shown in

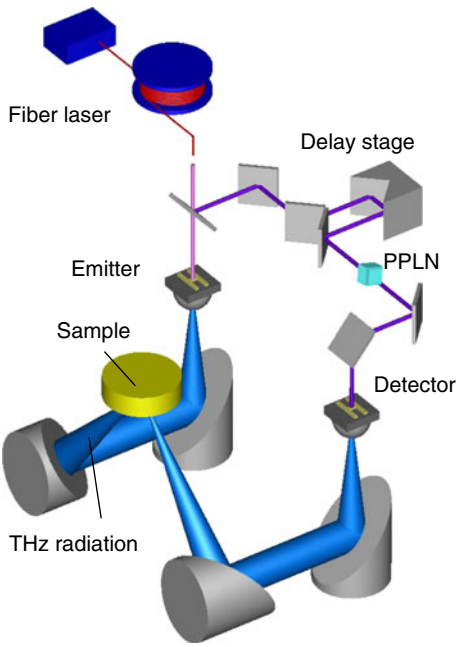

Fig. 1 Experimental set up of the THz imaging system

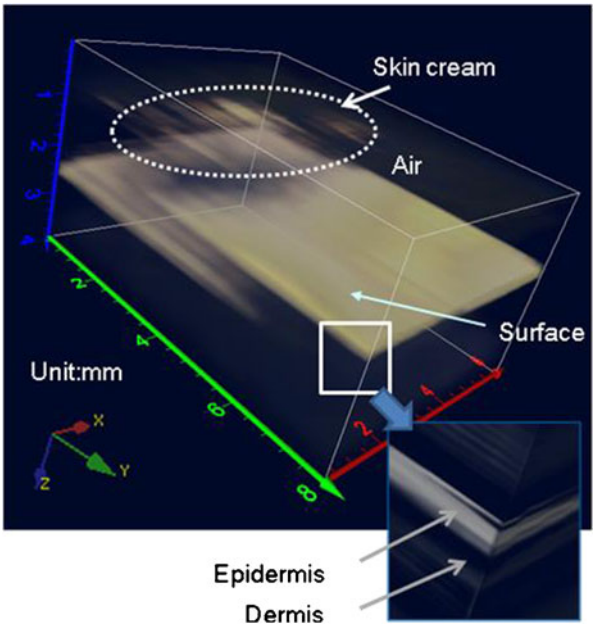

Fig. 2 Three-dimensional image of porcine skin. Skin cream was partially applied to the skin. Expanded cross sectional view around the surface is also shown

Fig. 3. Particular features were not recognized but the reflectance of tumor tissue was higher than that of normal tissue. The high reflectance of tumor tissue might be attributable to higher water contents or higher density of the cell nucleus. Figure 4(b) shows a two dimensional imaging of THz reflectance at 0.8 THz for a 10mm×13mm area. The tumor tissue is clearly discriminated thanks to its high reflectance. The corresponding light microscope image of the sample is shown in Fig. 4 (a). These results suggest the feasibility of THz clinical diagnosis based on tissues with no staining. The origin of this difference should be discussed with medical doctors and requires additional investigations.

2.2 Ridge waveguide THz generator

For further improvement of the above TDS system such as shorter acquisition time, a more efficient THz generator based on a ridge waveguide lithium niobate crystal was studied [33].

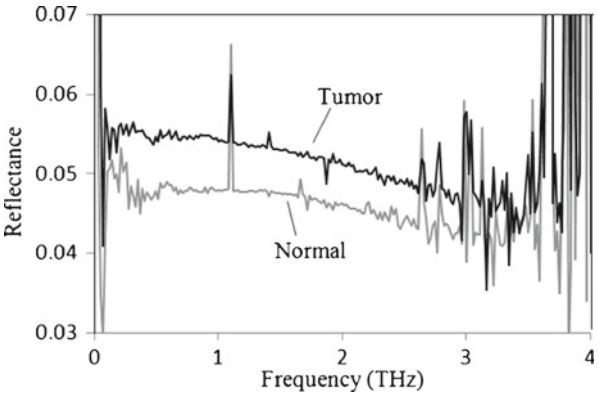

Fig. 3 Refractive indexes of paraffin embedded colorectal tissues calculated from THz-TDS measurement data. The refractive index of tumor tissue was higher than that of normal tissue

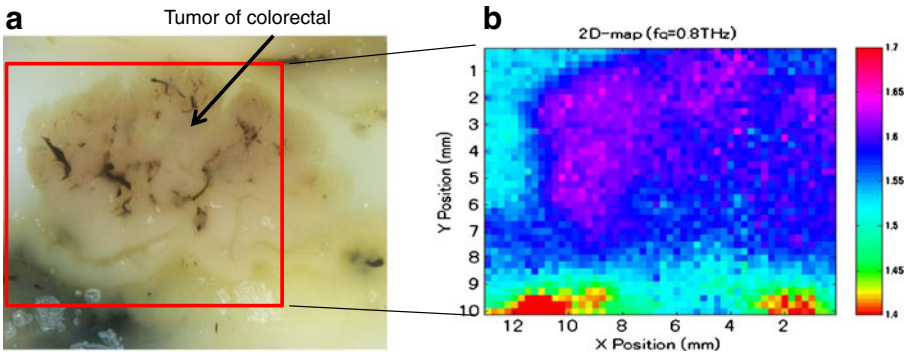

Fig. 4 Microscope image (a) and refractive index image at 0.8 THz (b) for a 10 mm×13 mm colorectal cancer block sample. The higher refractive index area, corresponding to the tumor tissue, is clearly discriminated against the normal tissue

The schematic structure of the ridge waveguide nonlinear generator is shown in Fig. 5. The waveguide is made of MgO-doped lithium niobate ($LiNbO_3$) with a 5-7 μm width and 3.8 μm thickness. As the optical power density in the waveguide can be very high, high conversion efficiency is expected by nonlinear optical effects based on the Cherenkov phase matched radiation. A conical Si prismatic coupler used to extract the THz emissions was placed on the waveguide using a thin polyethylene terephthalate (PET) buffer layer. In this experiment, an ultra-short pulse fiber laser with 34 fs pulse duration was used at 70 mW pump power.

Figure 6 (a) and (b) show the temporal waveform and the fast Fourier transform spectrum of the THz signal output from this device used as the emitter in the TDS system, respectively. The THz pulse duration is as short as 133 fs and the bandwidth of the spectrum reaches 7 THz in the upper limit. The total THz output power measured by a Si-bolometer was at least one hundred times larger than that of a conventional photoconductive antenna. Thus, this device has the potential to significantly improve the THz output power and bandwidth of TDS system. To this end, it is needed to optimize the shape of the Si prism according to the linear emission pattern of the waveguide.

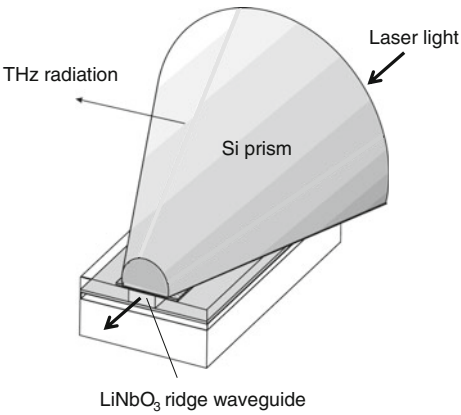

Fig. 5 Schematic structure of the ridge waveguide lithium niobate based THz generator with a Si conical prism

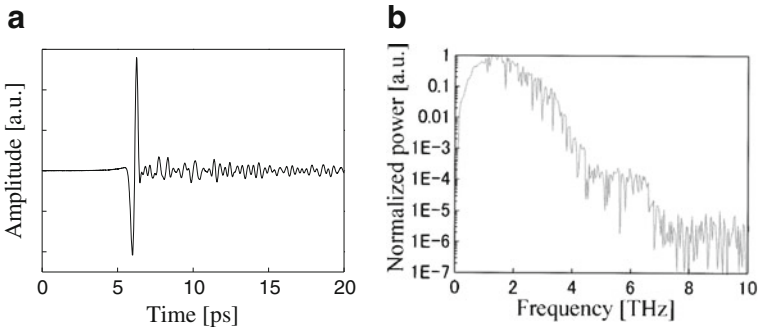

Fig. 6 THz temporal waveform (a) and corresponding Fourier spectrum (b) of the lithium niobate based THz generator. The THz pulse duration is 133 fs and the Fourier frequency extends to 7 THz

3 Semiconductor Based THZ Oscillators

To design THz imaging system the most important components are THz emitter and detector. Several excellent devices have been developed but the characteristics are not yet sufficient compared to optical devices. Namely, THz lasers similar to laser diodes and THz detectors similar to CMOS imaging devices are desirable in the near future. This leads to motivation for us to develop semiconductor based direct optical-electrical conversion devices with room temperature operation. As a THz source, RTD oscillators with a patch antenna were fabricated using an InGaAs/InAlAs/AlAs triple barrier structure [22].

3.1 RTD device structure

Figure 7 shows the scheme of a RTD oscillator with a patch antenna. We use an AlAs/InGaAs/InAlAs/InGaAs/AlAs (1.3/7.6/2.6/5.6/1.3 nm) triple-barrier RTD for the gain structure which showed a peak current density of 280 kA/cm^2 and a peak-valley-ratio of about 3 at R.T. A 2-steps post structure, which consist of a 0.2 μm thick RTD mesa on a 3 μm thick n^+-InGaAs layer (Si=1×10^{19}cm^{-3}), is buried in a 3 μm thick layer of benzo-cyclo-butene (BCB) and is sandwiched between a patch and a ground plane on InP substrates. The RTD mesa is set at a distance x from the center of the patch so as to tune the input impedance of the patch antenna. A λ/4 micro strip line for DC supply is connected to the center of the patch so as not to affect the resonant condition. A metal/BCB/metal structure serves as an on-chip metal-insulator-metal (MIM) capacitor and a bismuth film structure serves as a shunt resistor. Both are connected to the patch antenna through the micro strip line to suppress the parasitic oscillations due to resonances with the external bias circuit.

The oscillation frequency is basically determined by the resonant length of the patch L which is set to $\lambda_0/2\varepsilon_r^{1/2}$, where λ_0 is the oscillation wavelength in vacuum and ε_r is the relative permittivity of BCB. The actual oscillation frequency is shifted by the reactance component of the RTD, which originates from the transit delay of the triple-barrier and the depletion layer and the junction capacitance of the triple-barrier structure as well as the other parasitic elements. To increase the oscillation frequency of the RTD oscillator with patch antenna, the area of RTD mesa corresponding to the parasitic capacitance of RTD or the resonant length of patch L should be reduced. We utilize a small area RTD mesa of 2 μm in diameter to reduce the capacitance while keeping enough negative differential conductance (NDC) to satisfy the oscillation conditions. However, there is a trade-off between the area

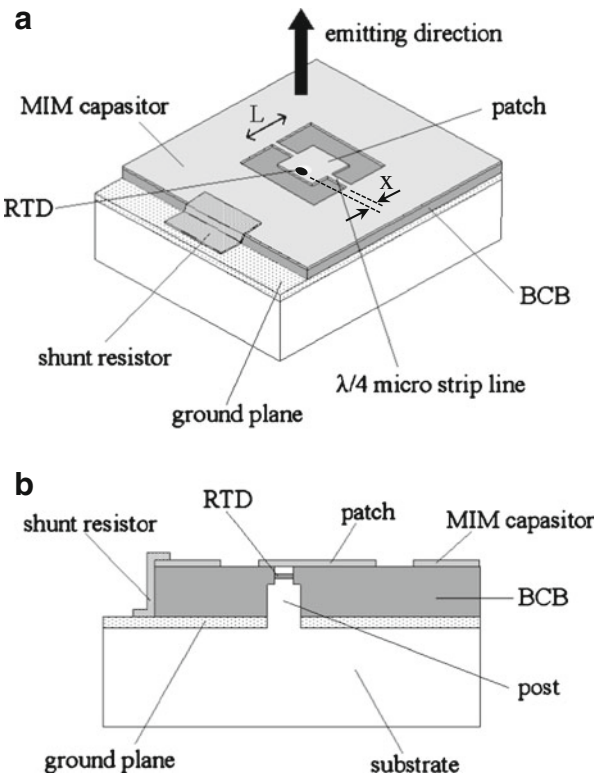

Fig. 7 Schematic of a RTD oscillator with an integrated patch antenna. (a) Perspective view; (b) cross-sectional view

and the thickness of the RTD mesa. A thick mesa structure of small diameter causes a non-negligible self inductance and series resistance although the thick BCB layer is effective to reduce the radiation loss of the patch antenna. Therefore, we adopt the 2-steps post structure shown in Fig. 7 (b), which consists of a RTD mesa of 2 μm diam. as the first step and n^+-InGaAs post of 16 μm diam. as the second step.

3.2 RTD oscillation characteristics

The output power and spectra were measured using a liquid He cooled Si composite bolometer and a Fourier transformed infrared (FT-IR) spectrometer. The device operated at R.T. under pulsed condition with lock-in technique to eliminate the noise of the bolometer (repetition frequency: 230 Hz, duty: 50%). Oscillations from 1.02 to 1.40 THz were observed when the diameter of RTD mesa was 2 μm and the resonant length of patch L was 50 μm [23], which are indicated as three open square points in Fig. 8. An example of measured FT-IR spectra is shown in inset of Fig. 8. The highest oscillation frequency of 1.40 THz was measured with a square patch of L= 50 μm and x= 5 μm. The output power was estimated to be less than 0.1 μW. Several satellite peaks were also observed around the main THz oscillation. They are assumed to be the harmonics of a spurious oscillation at the low frequency due to the parasitic elements.

The relationship between the oscillation frequency and the relative position of the RTD x/L is shown in Fig. 8. The solid line shows the analysis results which were calculated using the equivalent circuit of the RTD oscillator and the circuit parameters described in Ref. [22,

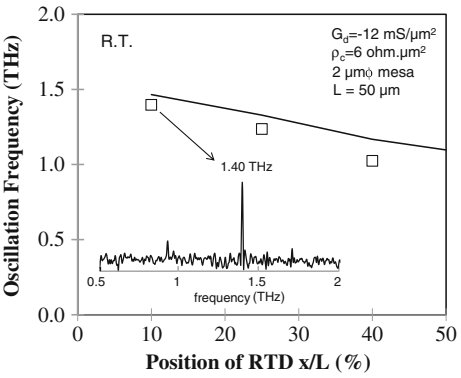

Fig. 8 Relationship between the oscillation frequency and the relative position of the RTD x/L. The antenna length L= 50 μm was fixed and the feed-point locations of the RTD x was varied from 20 μm to 5 μm. When x/L =10 %, the oscillation frequency was the highest at 1.4 THz. A frequency spectrum is showed in the inset of the graph

34]. The experimental results indicated by the open squares reasonably agree with our analysis. The slight difference between the experimental results and the analysis is supposed to be caused by the parasitic capacitance of the fabricated structure. From our analysis, the upper limit of the oscillation frequency is due to the insufficient NDC of our present RTD and the lower one is caused by the phase mismatch between the RTD and the antenna. In order to obtain higher frequency oscillations, it will be necessary to improve the device structure. For the RTD, it is effective to have a sufficient NDC, i.e., increasing the peak current density of the triple-barrier structure while keeping the peak valley-ratio. It is also important to reduce the loss caused by the parasitic elements such as the contact resistance.

4 Semiconductor Based THZ Detectors

Si-based SBD detectors have the potential to be integrated with CMOS devices, which will result in multi-pixel imaging devices. In order to obtain a response from Si devices in the THz range, a Schottky contact less than 1 μm was required. We successfully obtained over 1 THz detection signal by realizing submicron contacts using a KrF stepper with planar process [35].

4.1 SBD device structure and design

The structure of our Si based SBD detector is shown in Fig. 9. An SBD island consists of p-Si (t=60 nm) / p+Si (t=415 nm) epitaxial layer on a high resistivity Si substrate and a boron (acceptor) implanted region which reduces the contact resistance of ohmic contacts. Al electrodes are used for the Schottky contact with a diameter of 0.7 μm (the center of Fig. 9 (a)) and the ohmic contact (the right side of Fig. 9(a)). A log-periodic antenna placed on top of the SBD island is connected to the contacts via through-holes. The broadband log-periodic antenna as in ref. [36] is employed so as to characterize from sub-THz to 1 THz. We used about 1 μm-thick SiO_2 as a passivation film in order to prevent generating a stray capacitance between the antenna and the SBD island. The device was fabricated by photo lithography using a KrF stepper and dry etching.

Fig. 10 shows the equivalent circuit of the SBD and log-periodic antenna where R_a is the antenna's radiation resistance, R_s the series resistance of the SBD, and C_d the junction capacitance of the SBD. The ideal diode is depicted as the junction resistance R_d. We neglect the antenna reactance because the reactance of an ideal log-periodic antenna is zero. In this circuit, the THz power received by the antenna P_a transfers to the ideal diode. Thus, R_s and C_d

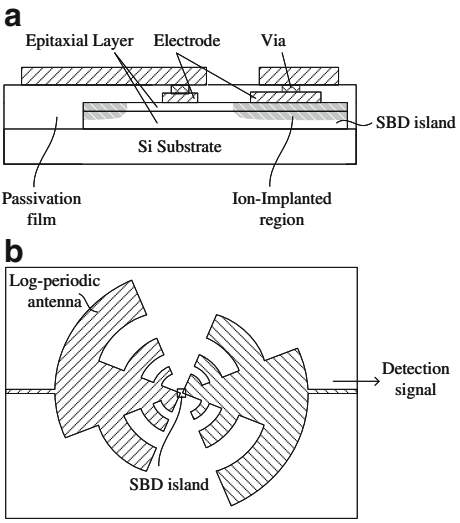

Fig. 9 Scheme of the SBD detector integrated with a log-periodic antenna. (a) Cross-sectional view of the device showing the SBD island on Si substrates; (b) top view of the device

are parasitic elements which must be minimized. If the parasitic elements can be neglected, the maximum transferred power P_d to the ideal diode is written as $P_{d,\max} = \frac{1}{2}|V|^2/4R_a$ where V is the amplitude of the equivalent voltage source. The factor of 1/4 is derived from the impedance matching of R_a and R_d. If the parasitic elements exist,

$$P_d = \frac{1}{2}|V|^2 \frac{R_d}{\{R_a + R_s + R_d\}^2 + \{\omega C_d R_d (R_a + R_s)\}^2} = P_{d,\max} \frac{4R_a R_d}{\{R_a + R_s + R_d\}^2 + \{\omega C_d R_d (R_a + R_s)\}^2}. \quad (1)$$

After the transfer, the THz power in the ideal SBD produces a rectified current [37]. The room temperature (300 K) current sensitivity related to the ideality n of the diode is S_I=19.2/n (A/W). Therefore, the current sensitivity including the impedance matching between the antenna and the SBD is written as (P_d/P_a) × S_I (A/W).

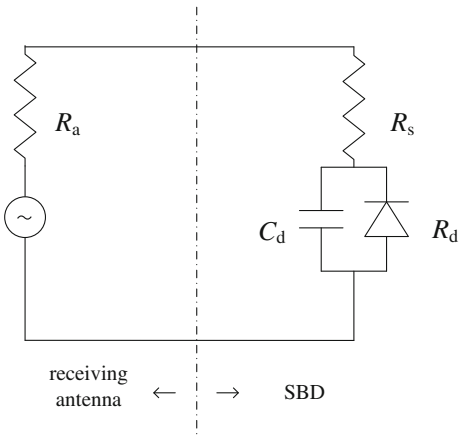

Fig. 10 Equivalent circuit of the SBD integrated with the log-periodic antenna as a receiving antenna

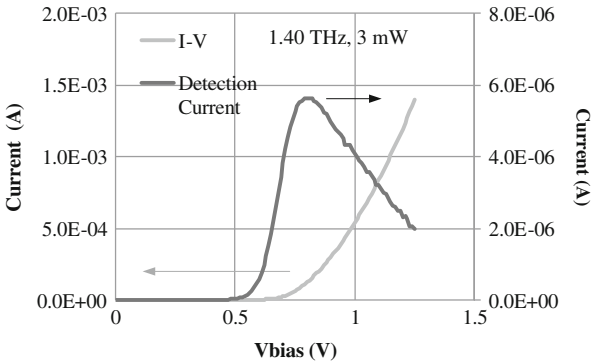

Fig. 11 Measured THz detection current under a 1.40-THz irradiation and corresponding I-V characteristics of the SBD detector

4.2 SBD detector characteristics

An example of experimental results of direct (video) detection is shown in Fig. 11. The rectified current between the SBD's electrodes was measured while irradiating the backside of the device with a mW-class THz gas laser (Coherent Inc.). The 1.04-THz and 1.40-THz stretching modes of the CH_2F_2 were chosen for the THz gas laser operation. In the THz optical path, a hemispherical Si lens with a radius of 15 mm in contact with the backside of the device was used. The detection current was simply derived from the differential measurement between the irradiation and dark cases. The detection current was maximized when the forward bias of the SBD was 0.8 V. The bias supply and the current monitoring were performed by a semiconductor parameter analyzer (HP 4155) and no lock-in technique was used. We obtained the current sensitivity by dividing the detection current by the irradiating THz power: 5.6 μA / 3 mW = 1.9 mA/W at 1.40 THz. The THz power was calibrated using a calorie meter (Scientech lnc.) .

Figure 12 shows the equivalent circuit analysis compared with the experimental results. We estimated that our 0.7 μm-diam SBD had about 2 f. of C_d and around 1000 Ω of R_d under 0.8-V applied bias. Current-voltage (I-V) characteristics denote that R_s amounts to a large value of 200 Ω because the contact resistance of the ohmic electrode was not optimized. According to electromagnetic simulations, the input impedance of the antenna is around 80 + j0 Ω and does not widely change between 0.2 THz and 2.5 THz. Assuming the above parameters, a theoretical current sensitivity (solid line in Fig. 12) including the impedance matching factor $(P_d/P_a)S_I$ decreases with -6 dB/octave due to the R_sC_d cut-off frequency around 0.3 THz. The measured current sensitivity at 1.04 THz and 1.40 THz are indicated as crosses in Fig. 12, which show the

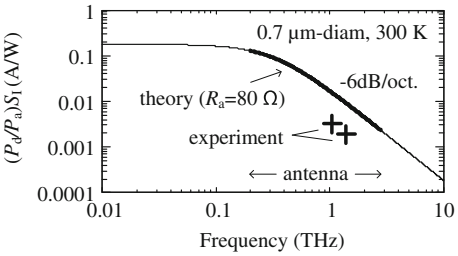

Fig. 12 Theorical and experimental frequency dependence of the current sensitivity of a 0.7μm-diam SBD detector at room temperature (300 K). The log-periodic antenna covers 0.2 THz to 2.5 THz. The coupling loss and miss alignment are not taken into account in the experimental results

same frequency dependence as the theory. For the sake of the completeness, we should take the coupling loss and miss alignment of the THz optics into consideration.

To compare these results with other SBD detectors, we have to convert the current sensitivity S_I to voltage sensitivity S_V using $S_I \cong R_d \times S_I(V/W)$ [25]. The derived voltage sensitivity including the impedance matching factor $(P_d/P_a)S_V$ of our Si based SBD detector is the order of 1 V/W around 1 THz which is 100 times smaller than recent III-V semiconductor based SBD detectors [27, 28]. In order to improve the sensitivity around 1 THz, the equivalent circuit analysis suggests that a smaller diameter Schottky electrode close to 0.3 μm is required. The reduction of R_s using Si technology is also crucial.

5 Conclusion

A THz imaging system including high efficient terahertz sources and detectors for medical applications was described. A fiber laser based THz-TDS system was developed and three-dimensional imaging of biological tissue was demonstrated. Differences in physical properties were observed between tumor tissues and normal tissues without relying on any staining.

For future THz biomedical imaging systems, improved THz sources and detectors are required. A ridge waveguide lithium niobate generator was designed for the TDS imaging system. A significantly higher THz pulse power than conventional photoconductive antenna was achieved by Cherenkov phase matching generation.

Concerning electronic source devices, resonant tunneling diode oscillators with a patch antenna were fabricated using an InGaAs/InAlAs/AlAs triple barrier structure. On the other side, Schottky barrier diode detectors with a log-periodic antenna were fabricated by thin-film technology on Si substrate. Both devices operate at 1.4 THz at room temperature. These devices are promising to expand THz medical imaging applications as well as inspections and telecommunications.

REFERENCES

1. Q. Wu and X.-C. Zhang, "Free-space electro-optics sampling of mid-infrared pulses," *Appl. Phys. Lett.* **71**, 1285 (1997).
2. C. Kübler, R. Huber, S Tübel, and A. Leitenstorfer, "Ultrabroadband detection of multi-terahertz field transients with GaSe electro-optic sensors: Approaching the near infrared," *Appl. Phys. Lett.* **85**, 3360 (2004).
3. Y. C. Shen, P. C. Updhya, H. E. Beere, E. H. Linfield, A. G. Davies, I. S. Gregory, C. Baker, W. R. Tribe, and M. J. Evans, "Generation and detection of ultrabroadband terahertz radiation using photoconductive emitters and receivers," *Appl. Phys. Lett.* **85**, 164 (2004).
4. S. Kono, M. Tani, P. Gu, and K. Sakai, "Detection of up to 20 THz with a low-temperature-grown GaAs photoconductive antenna gated with 15 f. light pulses," *Appl. Phys. Lett.* 77, 4104 (2000).
5. J. Takayanagi, H. Jinno, S. Ichino, K. Suizu, M. Yamashita, T. Ouchi, S. Kasai, H. Ohtake, H. Uchida, N. Nishizawa, and K. Kawase, "High-resolution time-of-flight terahertz tomography using a femtosecond fiber laser," *Opt. Express* **17**, 7533 (2009).
6. A. J. Fitzgerald, V. P. Wallace, M. J-Linan, L. Bobrow, R. J. Pye, A. D. Purushotham, and D. D. Arnone, "Terahertz pulsed imaging of human breast tumors," *Radiology* **239**, 533 (2006).
7. E. Jung, M. Lim, K. Moon, Y. Do, S. Lee, H. Han, H. Choi, K. Cho, and K. Kim, "Terahertz Pulse Imaging of Micro-metastatic Lymph Nodes in Early-stage Cervical Cancer Patients," *J. Optical Society of Korea* **15**, 155 (2011).
8. C. A. Lieber, S. K. Majumder, D. L. Ellis, D. D. Billheimer, and A. M-Jansen, "In Vivo Nonmelanoma Skin Cancer Diagnosis Using Raman Microspectroscopy," *Lasers in Surgery and Medicine* **40**, 461 (2008).

9. C. Hua, M. Shi-Hua, Y. Wen-Xing, W. Xiu-Mei[1], W. Xiao-Zhou, "The Diagnosis of Human Liver Cancer by using THz Fiber-Scanning Near-Field Imaging," *Chin. Phys. Lett*. **30**, 030702 (2013).
10. A. M. Hassan, D. C. Hufnagle, M. El-Shenawee1 and G. E. Pacey., "Terahertz imaging for margin assessment of breast cancer tumors," Microwave Symposium Digest (MTT), IEEE MTT-S International (2012).
11. J. Hebling, K.-L. Yeh, M. C. Hoffmann, B. Bartal, and K. A. Nelson, "Generation of high-power terahertz pulses by tilted-pulse-front excitation and their application possibilities," *J. Opt. Soc. Am. B* **25**, B6 (2008).
12. K. Suizu, K. Koketsu, T. Shibuya, T. Tsutsui, T. Akiba, K. Kawase, "Extremely frequency-widened terahertz wave generation using Cherenkov-type radiation," *Optics Express* **17**, 6676 (2009).
13. K. Takeya, K. Suizu, H Sai, T. Ouchi, and K. Kawase, "Wide spectrum Terahertz-wave generation from nonlinear waveguides" IEEE J. Sel. Top. Quant. Electron. **19**, 8500212 (2013).
14. J. Faist, F. Capasso, D. L. Sivco, C. Sirtori, A. L. Hutchinson, and A. Y. Cho, "Quantum Cascade Laser", *Science* **264**, 553 (1994).
15. E. R. Brown, J. R. Sonderstrom, C. D. Parker, L. J. Mahoney, K. M. Molvar, and T. C. McGill, "Oscillations up to 712 GHz in InAs/AlSb resonant–tunneling diodes," *Appl. Phys. Lett*. **58**, 2291 (1991).
16. W. Hafez, W. Snodgrass, and M. Feng (2005), "12.5 nm base pseudomorphic heterojunction bipolar transistors achieving f_T=710 GHz and f_{MAX}=340 GHz," *Appl. Phys. Lett*. **87**, 252109 (2005).
17. V. Jain, E. Lobisser, A. Baraskar, B. J. Thibeault, M. J. W. Rodwell, Z. Griffith, M. Urteaga, D. Loubychev, A. Snyder, Y. Wu, J. M. Fastenau, and W. K. Liu, "InGaAs/InP DHBTs in a dry-etched refractory metal emitter process demonstrating simultaneous f_t/f_{max} ~ 430/800 GHz," *IEEE Trans. Electron. Devices* **32**, 24 (2011).
18. E. Ojefors, B. Heinemann, U.R. Pfeiffer, "Active 220- and 325-GHz frequency multiplier chains in an SiGe HBT technology, " *IEEE Trans. Microw. Theory Tech*. **59**, 1311 (2011).
19. S. Suzuki, M. Asada, A. Teranishi, H. Sugiyama and H. Yokoyama, "Fundamental oscillation of resonant tunneling diodes above 1 THz at room temperature", *Appl. Phys. Lett*. **97**, 242102 (2010).
20. H. Kanaya, H. Shibayama, R. Sogabe, S. Suzuki, and M. Asada, *"Fundamental Oscillation up to 1.31 THz in Resonant Tunneling Diodes with Thin Well and Barriers," Appl. Phys. Express* **5**, 124101 (2012).
21. M. Feiginov, C. Sydlo, O. Cojocari, and P. Meissner, "Resonant-tunnelling-diode oscillators operating at frequencies above 1.1 THz," *Appl. Phys. Lett.* **99**, 233506 (2011).
22. R. Sekiguchi, Y. Koyama, and T. Ouchi, "Subterahertz oscillations from triple-barrier resonant tunneling diodes with integrated patch antennas", *Appl. Phys. Lett.* **96**, 062115 (2010).
23. Y. Koyama, R. Sekiguchi, and T. Ouchi, "Oscillations up to 1.40 THz from Resonant Tunneling Diode Based Oscillators with Integrated Patch Antenna", *Appl. Phys. Express* **6**, 064102 (2013).
24. K. Mizuno, R. Kuwahara, and S. Ono, "Submillimeter detection using a Schottky diode with a longwire antenna," *Appl. Phys. Lett.* **26**, 605 (1975).
25. K. B. Cooper, R. J. Dengler, G. Chattopadhyay, E. Schlecht, J. Gill, A. Skalare, I. Mehdi, and P. H. Siegel, "A High-Resolution Imaging Radar at 580 GHz," *IEEE Microw. Wireless Compon. Lett,* **18**, 64 (2008).
26. E. R. Brown, A. C. Young, J. Zimmerman, H. Kazemi, and A. C. Gossard, "Advances in Schottky rectifier performance," *IEEE Microwave magazine* **8**, 54 (2007).
27. J. L. Hesler, T. W. Crowe, "NEP and responsivity of THz zero-bias Schottky diode detectors," in *Proc. Joint 32nd International Conference on Infrared and Millimeter Waves, 2007 and the 2007 15th International Conference on Terahertz Electronics. IRMMW-THz. Sept. 2007*, p. 844 (2007).
28. H. Ito, F. Nakajima, T. Ohno, T. Furuta, T. Nagatsuma, and T. Ishibashi, "InP-Based Planar-Antenna-Integrated Schottky-Barrier Diode for Millimeter- and Sub-Millimeter-Wave Detection," *Jpn. J. Appl. Phys.* **47**, 6256 (2008).
29. T. Watanabe, S. B. Tombet, Y. Tanimoto, Y. Wang, H. Minamide, H. Ito, D. Fateev, V. Popov, D. Coquillat, W. Knap, Y. Meziani, T. Otsuji, "Ultrahigh sensitive plasmonic terahertz detector based on an asymmetric dual-grating gate HEMT structure," *Solid-State Electronics* **78**, 109 (2012).
30. F. Schuster, D. Coquillat, H. Videlier, M. Sakowicz, F. Teppe, L. Dussopt, B. Giffard, T. Skotnicki, and W. Knap, "Broadband terahertz imaging with highly sensitive silicon CMOS detectors," *OPTICS EXPRESS* **19**, 7827 (2011).
31. S. Boppel, A. Lisauskas, M. Mundt, D. Seliuta, L. Minkevicius, I. Kasalynas, G. Valusis, M. Mittendorff, S. Winnerl, V. Krozer, H. G. Roskos, "CMOS Integrated Antenna-Coupled Field-Effect Transistors for the Detection of Radiation From 0.2 to 4.3 THz ," *Digital Object Identifier* **60** , 3834 (2012).
32. H. Ruonan, Z. Yaming, D. Coquillat, H. Videlier, W. Knap, E. Brown, K.K. O, "A 280-GHz Schottky Diode Detector in 130-nm Digital CMOS ," EEE J. Solid-State Circuits **46**, 2602 (2011).
33. S. Fan, H. Takeuchi, T. Ouchi, K. Takeya, K. Kawase, "Broadband terahertz wave generation from a MgO:$LiNbO_3$ ridge waveguide pumped by a 1.5-μm femtosecond fiber laser", *Opt. Lett.* **38**, 1654 (2013).

34. M. Asada, S. Suzuki, and N. Kishimoto, "Resonant Tunneling Diodes for Sub-Terahertz and Terahertz Oscillators", *Jpn. J. Appl. Phys*. **47**, 4375 (2008)
35. R. Sekiguchi and T. Ouchi, "Above 1 THz detection using silicon based Schottky barrier diodes," *in Proc. International Symposium on Frontiers in THz Technology (FTT)2012*,. Pos1.22 (2012).
36. H. Saijo, M. Morimoto,T. Kiwa, and M. Tonouchi, "Terahertz emission properties from YBCO thin film log-periodic antennas," *Physica C* 362 319 (2001).
37. H. C. Torry and C. A. Whitmer, Crystal Rectifiers, vol. 15 of MIT Radiation Laboratory Series (McGraw-Hill, New York 1948).